RSC Advances

PAPER

View Article Online
View Journal | View Issue

Cite this: RSC Adv., 2014, 4, 25461

Self-assembled peptide nanotubes as potential nanocarriers for drug delivery†

Qinrong Wang,[a] Xin Zhang,*[a] Jinhong Zheng[b] and Daojun Liu*[b]

Received 12th April 2014
Accepted 27th May 2014

DOI: 10.1039/c4ra03304c

www.rsc.org/advances

The self-assembly of amphiphilic peptide I_3K (Ac-I_3K-NH_2) and its potential application as a drug nanocarrier have been investigated. I_3K monomers and nanotubular segments were initially the dominant species in aqueous solution and they gradually self-assembled into mature nanotubes with heights of approximately 12 nm and lengths of more than 1 μm. The encapsulation properties of the self-assembled peptide nanotubes were then investigated using model compound guests, including anionic hydrophilic methyl orange (MO) and hydrophobic oil red. It revealed that the model compounds could be efficiently encapsulated by I_3K assemblies *via* electrostatic and hydrophobic interactions, respectively. Atomic force microscopy images demonstrated that variations in drug concentration did not significantly alter the structures of the peptide assemblies but could affect their sizes. Circular dichroism analyses indicated the predominance of β-sheet conformation associated with the self-assembled system regardless of drug concentrations. The *in vitro* releasing behavior of the encapsulated model drugs was also studied by the techniques of dialysis. The entrapped model drug MO exhibited an accelerated release as the solution pH was either decreased to 2.0–3.0 or increased to 10.0–11.0 but revealed a sustained release at physiological pH. These results demonstrated that these self-assembled peptide nanotubes could serve as potential drug nanocarriers with efficient encapsulation ability, and sustained and pH-responsive release properties.

1. Introduction

Effective drug delivery systems are necessary to achieve sufficient drug bioavailability and facilitate clinical use because these systems can reduce side-effects by targeting drugs to required pathological sites in the body and controlling drug release; these systems can also increase the bioavailability of drugs by increasing drug solubility and protecting drug molecules from degradation.[1–4] Ideal drug delivery materials should satisfy the following requirements: non-toxicity; good biocompatibility; high stability; suitable mechanical strength; controlled release of the active ingredients; and ease in incorporating bioactive factors.[5,6] Several types of materials, including vesicles (liposomes), amphiphilic gels, polyelectrolyte capsules, nanodisks, and colloidosomes, have been used to carry various drugs. However, these carrier types fail to satisfy all of these requirements, and the encapsulation of drugs by nanostructures remains unclear.[1,7]

Over the past few years, molecular self-assembly has extensively evolved as a promising approach to fabricate biomimetic nanostructures and macroscopic functional biomaterials with high levels of biocompatibility, biodegradability, chemical modifiability, and great efficiency.[8–12] Molecular self-assembly process is the spontaneous association of individual components to form well-defined structures and generally controlled by the exquisite combination of non-covalent interactions.[13,14] The interactions are relatively weak in isolation; nevertheless, such interactions can be combined to generate a diverse array of nanostructures. Self-assembled peptides have emerged as biomaterials that can potentially outperform other drug delivery systems. The use of self-assembled nanocarriers (*e.g.*, hydrogels, micelles, and multilayer capsules) has drawn great attention because of their good pharmacological properties in drug delivery applications.[15,16] Previous studies reported that self-assembled peptides can stabilize small molecules (*e.g.*, pyrene, proteins, and hydrophobic anticancer agents) in aqueous solution; as such, these peptides can be used as effective drug delivery carriers.[12,17–19] However, the isolation and purification of long-chain polymers are costly and laborious. Hence, short amphiphilic peptides, with hydrophilic/hydrophobic compartments, specific conformations, and well-defined self-assembled nanostructures, have been gained attention as a new class of self-assembled molecules.[20–23]

Self-assembled materials formed from short amphiphilic peptides exhibit great potential in various biotechnological applications, such as biomineralization, tissue engineering,

[a]Department of Chemistry, Shantou University, Shantou 515063, PR China. E-mail: xzhang@stu.edu.cn

[b]Medical College, Shantou University, Shantou 515041, PR China. E-mail: liudj@stu.edu.cn

† Electronic supplementary information (ESI) available. See DOI: 10.1039/c4ra03304c

antibacterial application, and membrane protein stabilization, because of several advantages; these advantages include easy sequence modification, controllable morphologies, inherent bioactivity, and specific binding to metal ions.[9,23–26] Xu *et al.* studied the anticancer activities of A_9K peptide and found that it could strongly inhibit the growth of human promyelocytic leukemia HL_{60} cells and cancerous Hela cells, while keeping benign to the host cells.[26] Our previous self-assembled and biomimetic investigation also revealed that short amphiphilic peptides exhibit higher stability and mechanical strength than other peptides.[27,28] These amphiphilic peptides can spontaneously organize themselves into nanostructures that exhibit biocompatibility and improved stability; thus, such peptides may supply a stable and protected environment for drugs and facilitate active targeting. However, short amphiphilic peptides used for drug delivery are limited. Therefore, unique amphiphilic structures and desirable characteristics of short amphiphilic peptide self-assemblies indicate that these materials can be used as effective nanomaterials for the encapsulation of hydrophilic/hydrophobic drugs and for controlled drug release.[6] In addition, the tubular shape of nanoparticles can be considered in similar applications because this shape allows an efficient functionality of their inner and outer surfaces; in this way, nanotubes can be developed to facilitate drug loading, biorecognition, and biocompatibility.[29]

In this study, efforts were devoted to exploit the self-assembly of short amphiphilic peptide I_3K (Ac-IIIK-NH_2) as potential drug delivery systems with efficient encapsulation and sustained release. The short amphiphilic peptide in aqueous solution can readily self-assemble into β-sheet-rich nanotubes with hydrophilic and charged residues outside the layer *via* hydrophobic interaction and hydrogen bonding. β-sheet nanostructures are stable in the presence of organic agents (ethanol, acetonitrile, and acetone), anions (carbonate, sulfate, and phosphate anions), and silicic acid.[22,28] Self-assembled I_3K peptide nanotubes can solubilize hydrophobic drugs in solution *via* hydrophobic interactions. Furthermore, these peptide molecules contain a lysine terminal whose side-chain charge can be easily altered by regulating the solution pH. Therefore, self-assembled peptides can encapsulate hydrophilic drugs *via* electrostatic interactions at neutral pH. As pH is decreased to change the charges of entrapped drugs or as pH is increased to deprotonate lysine, the pH-responsive release of entrapped drugs occurs. The self-assembled nanotubes from short I_3K could be used as potential drug carrier for hydrophilic and/or hydrophobic compounds. The results provided a versatile method to improve our knowledge on the function of peptide structures in controlled drug delivery systems *in vitro*.

2. Experimental section

2.1 Materials

Protected amino acids (Fmoc-L-Ile-OH and Fmoc-L-Lys(Boc)-OH), *O*-(1*H*-benzotriazole-1-yl)-*N*,*N*,*N*′,*N*′-tetramethyluronium hexafluorophosphate (HBTU), *N*-hydroxybenzotriazoleanhydrous (HOBt anhydrous), and *N*,*N*′-diisopropyl ethylamine (DIEA) for peptide synthesis were purchased from GL Biochem, Ltd (Shanghai, China). Methyl orange (MO) and oil red (OR) were obtained from Alfa Aesar. Other reagents and solvents were purchased from Sigma-Aldrich and used as received. Dichloromethane (DCM) and dimethylformamide (DMF) were re-distilled and subsequently dried with molecular sieves prior to peptide synthesis. Cellulose dialysis tubing (MWCO; 14 kDa) was purchased from Jingkehongda Biotechnology Co. (China). Water was processed by a Millipore water purification system with a minimum resistivity of 18.0 MΩ cm.

2.2 Sample characterization

Nanoscope IIIa Multimode atomic force microscope (AFM; America Digital Instrument Co.) measurements was performed in a tapping mode to characterize the morphology and size of self-assembled peptide, MO–peptide, and OR–peptide colloids. All of the samples were probed with a TESP silicon probe (Veeco, Santa Barbara, CA) with a nominal spring constant of 42 N m^{-1} and a typical frequency of 300 kHz. To prepare the sample, we deposited 10 μL of peptide solutions onto freshly cleaved mica surfaces. After 20 s, the excess liquid was removed from the mica surface and then gently dried with a weak stream of N_2. After the sample was prepared, the mica surface was immediately subjected to AFM imaging. Images were collected at a scan rate of 1 Hz and a scan angle of 0°. Topographic data were regularly recorded as 512×512 pixel images simultaneously in trace and retrace directions to check for scan artifacts. Image analysis was conducted using the Digital Instruments Nanoscope software (version V530r3sr3). All of the images were flattened using a first-order line fit to collect piezo-derived differences between scan lines. Circular dichroism (CD) spectra were recorded on an MOS 450 spectrophotometer (Biologic, France) in a 1 mm quartz cell. The wavelength-dependent CD spectra were recorded from 180 nm to 250 nm (at a rate of 50 nm min^{-1}) at each nanometer with a bandwidth of 1 nm. Each spectrum was an average of three accumulations and smoothed by adjacent averaging. The resultant CD signals were expressed as $[\theta] \times 10^{-3}$ degrees square centimeters per decimole. Ultraviolet-visible (UV-Vis) absorption spectra were recorded on a UVPC 2501 spectrophotometer (Shimadzu). All of the samples were prepared in triplicates.

2.3 Peptide synthesis

The short amphiphilic peptide I_3K (I, isoleucine; K, lysine) was synthesized on a CEM liberty microwave synthesizer according to the general procedure of Fmoc chemistry of solid-phase peptide synthesis.[22,30,31] Rink amide resin was used to enable C-terminal amidation. The N-terminus was capped with acetic anhydride before this terminal was cleaved from the resin; as a result, a molecule with only one positive charge from the side chain of the lysine residue was formed at neutral pH. Fmoc-deprotection reactions were performed with 20% piperidine and 0.1 M HOBt in DMF solution. Coupling and N-terminal capping reactions were catalyzed with a mixture of HBTU–HOBt–DIEA. Cleavage from the resin and deprotection of the protecting groups on the side-chains were performed using a mixture of trifluoroacetic acid, triisopropylsilane, H_2O, and ethanedithiol at a ratio of 94 : 1 : 2.5 : 2.5. The crude products dissolved in DCM were rotary evaporated to a concentrated solution. The cleaved peptides were then purified by depositing with copious cold ether at least six times and centrifuged until the pH was constant at approximately 6. Afterward, the final peptide products were lyophilized for 2 days to reach >95% purity as assessed by reverse-phase high-performance liquid chromatography (RP-HPLC; Fig. S1, ESI†) and electrospray-ionization mass spectrometry (ESI-MS; Fig. S2, ESI†). The measurements were performed using Waters 2695 Alliance HPLC system (Shiseido C18 column, 4.6 mm × 250 mm) and Finnigan Mat TSQ 7000 instruments.

2.4 Preparation of peptide self-assembly

Peptide self-assembly was prepared by directly dissolving the dry samples in pure water until no detectable precipitates were observed. The pH values of the as-prepared peptide solutions were slightly adjusted to approximately 7 by adding a minimum amount of either diluted NaOH or HCl solution. The peptide stock solution was incubated for at least one week at room temperature before characterization was performed.

2.5 Determination of the loading capacity of model drugs by the dialysis method

The encapsulation of anionic hydrophilic MO (structure shown in Fig. 1a) by the peptide self-assembly was conducted using the membrane dialysis method.[32] MO (32.5 mg mL^{-1}) was added to the self-assembled peptide solution (4 mL). The solution was then sonicated for 15 min at room temperature. Afterward, the clear solution was thoroughly dialyzed against water (100 mL) under sink conditions to remove free MO. Free MO in the absence of peptide solution was also dialyzed under similar conditions and used as a control sample. The amount of MO in the dialysate was characterized using a UV-Vis spectrophotometer and subsequently subtracted from the total amount of added MO to obtain the loading capacity of self-assembled peptide.

To encapsulate hydrophobic OR, an excess of OR (structure shown in Fig. 1b) solid was added to the self-assembled peptide solution (4 mL). The resulting mixture was vigorously and continuously stirred at room temperature for 2 days. The residual OR was removed by centrifugation (14 000 rpm) for 20 min. The obtained clear supernatant was then characterized using a UV-Vis spectrophotometer to determine the corresponding absorbance. The amounts of OR solubilized in the peptide solution were determined using a calibration curve constructed from the standard solution of OR in THF.

2.6 Release of MO from peptide self-assembly

The release of MO from I_3K self-assemblies was investigated according to the dialysis method at room temperature by using a model compound-loaded peptide solution (4 mL) against water (100 mL) under varying pH conditions (pH 2.0 to 11.0).[32] The model compound-loaded peptide solution was prepared as described in Section 2.5. No buffer system can be used to cover such a wide pH range; hence, the pH values of the releasing system were adjusted using HCl or NaOH. A certain volume of the release media was withdrawn at specific time intervals, and an equal volume of fresh release media was added to replenish the reaction. The amounts of released model drug were characterized using a UV-Vis spectrophotometer.

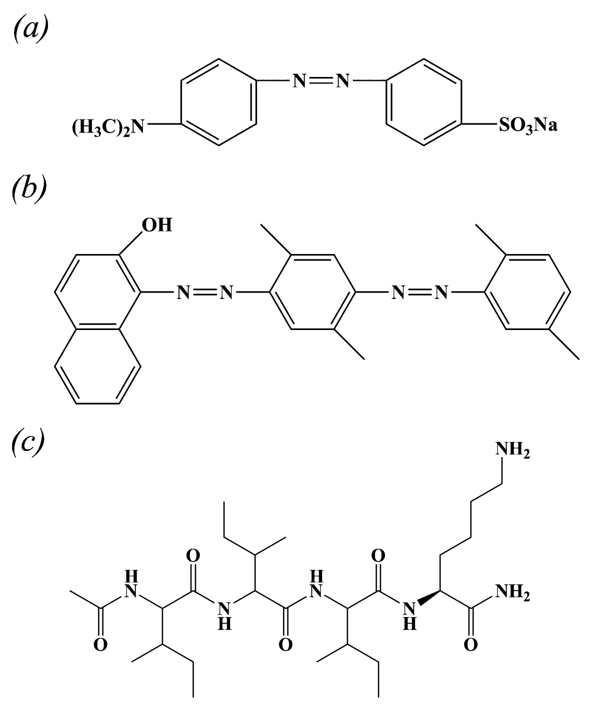

Fig. 1 Molecular structures (a) MO, (b) OR, and (c) I_3K.

3. Results and discussion

3.1 Self-assembly of I_3K peptide

The basic molecular structure of the short amphiphilic peptide I_3K used in this study is shown in Fig. 1c. The peptide consists of one lysine residue at the C-terminus acting as the hydrophilic tail and three isoleucine residues at the N-terminus acting as the hydrophobic segment. Such a unique arrangement of amino acids can induce the amphiphilic character of I_3K molecules.

Peptide self-assembly is the spontaneous organization of peptide molecules into complex supramolecular structures. The structure and size of self-assembled nanostructures are primarily determined by the subtle balances between non-covalent interactions (hydrophobic interactions, intermolecular or intramolecular hydrogen bonding, van der Waals forces, and electrostatic interactions).[12,13] Peptides are known to self-assemble into nanostructures over time.

Peptide monomers and tubular segments are initially the dominant species in aqueous solution; long and short nanotubes coexisted. Most of the self-assembled nanostructures exhibit a propensity for twisting (Fig. 2a). As incubation time is extended, small peptide fragments likely integrate into cylindrical nanotubes, primarily growing along the direction of hydrogen bonding (Fig. 2b). The amount of peptide nanotubes

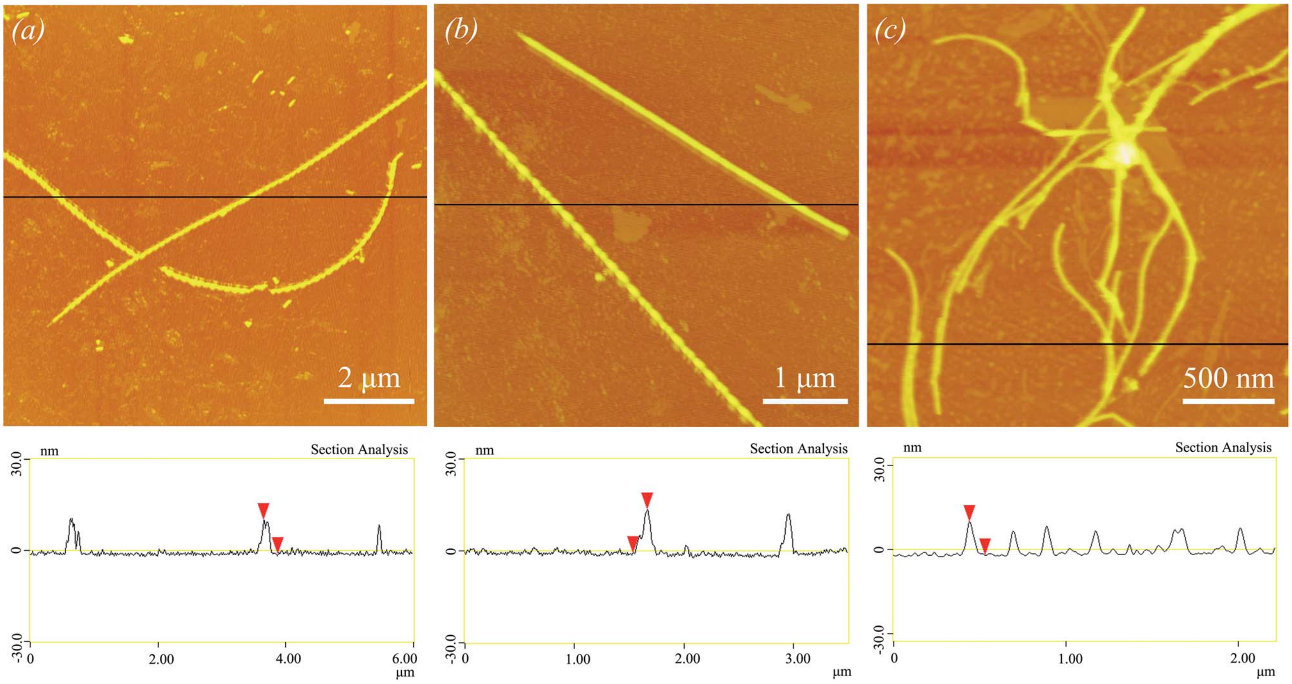

Fig. 2 AFM height images of I_3K self-assemblies (3 mM at pH 7.0) at different time points: (a) 2 days, (b) 4 days, and (c) 7 days.

with dimensions of approximately 11.2 nm in width also increased as incubation time was prolonged; however, gaps or joints can be observed in the helical structures. At the early self-assembled stage of lipids and amphiphilic peptides, helical nanostructures are generally present and considered as intermediate structures during the growth of tubular self-assemblies.[33–36] As the incubation time was further extended to one week, the twisting force became more intensified along the main axis and triggered the edges of the helical nanostructures to grow into well-ordered and highly homogeneous nanotubes with a smooth outer surface. No further variation in the morphology of I_3K nanotubes occurred over time, demonstrating that the self-assembly process reached equilibrium (Fig. 2c). On the basis of the corresponding AFM sectional profiles and transmission electron microscopy image (Fig. S3, ESI†), it was found that the uniform nanotubes formed by I_3K were approximately 12 nm in diameter and several micrometers in length. Although lengths vary, the diameters of these nanotubes are rather narrowly distributed.

Inspired by the work of Xu,[37] the dynamic self-assembly process of I_3K was proposed (Fig. 3). During the initial stage of I_3K peptide self-assembly process, I_3K molecules aggregated into small peptide segments that are composed of interdigitated bilayers and then self-assembled into short nanotubular segments. Peptide monomers are also present and then gradually grow into mature nanotubes. The lateral growth is primarily induced by the hydrophobic interactions among isoleucine side chains. Self-assembly achieves balance by surface curving, molecular chirality, hydrogen bonding, and electrostatic repulsion between surface lysine residues. Once peptide self-assembly occurs, hydrophilic lysine residues are distributed on both sides of the surface of the self-assembled nanotubes and become exposed to water; by comparison, hydrophobic isoleucine residues are retained in the interior. These results are consistent with those in previous studies, in which changes from thin ribbons to nanotubes are reminiscent of this phenomenon, and ribbon structures are considered as precursors during the growth of tubes.[37–41]

3.2 Encapsulation properties of I_3K self-assemblies

Self-assembled peptides show great potential applications in tissue engineering and controlled drug delivery because of their good biocompatibility, versatile synthetic pathway, and excellent chemical stability.[42–44] Under physiological pH, self-assembled I_3K nanotubes possess positively-charged lysine outer and inner surfaces and a hydrophobic interior, and therefore, these self-assemblies could not only entrap negatively-charged guest molecules *via* electrostatic interactions but also solubilize hydrophobic compounds *via* hydrophobic interactions (Fig. 3). To investigate the encapsulation property of the I_3K self-assembled peptide nanotubes, MO and OR were used as anionic hydrophilic and hydrophobic model drugs, respectively. The encapsulation of model drugs by self-assembled nanotubes was performed in water, and the loading capacities of both model drugs were characterized by UV-Vis spectroscopy (Fig. 4).

The UV-Vis spectra of MO entrapped in the self-assembled peptides showed a decrease in absorption peaks and a small shift in the wavelength of maximum absorption ($\lambda_{max} = 459$ nm) compared with those of free MO molecules ($\lambda_{max} = 464$ nm) (Fig. 4a). This result could be attributed to the formation of MO dimers once the MO molecules were close with one another as these molecules were entrapped by self-assembled peptide

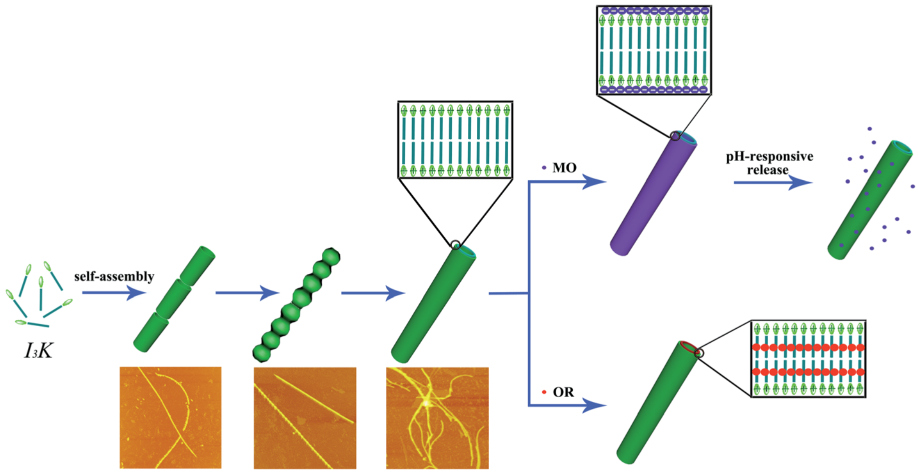

Fig. 3 Schematic of the dynamic self-assembly of I_3K peptide and its application in controlled drug delivery systems *in vitro*.

nanotubes. The UV-Vis absorbance measurements demonstrated that MO could be efficiently entrapped by the self-assembled I_3K with a high loading capacity and high temporal stability. The loading capacity expressed in mass ratio of encapsulated MO guest to I_3K host (m_{guest}/m_{host}) was estimated to be 12%. The loading capacity expressed in molar ratio of encapsulated MO guest molecules to I_3K host (n_{guest}/n_{host}) was calculated to be 0.2. Similarly, the UV-Vis spectra of OR encapsulated by the self-assembled peptides also revealed a small shift in the wavelength of maximum absorption ($\lambda_{max} = 514$ nm) than that of free OR ($\lambda_{max} = 517$ nm; Fig. 4b). The result also revealed that the hydrophobic model compound OR can be solubilized in the solution of self-assembled peptide.[45] The loading capacity of OR can reach up to 8% (w/w), and the relative solubility of pyrene increased up to 100-fold relative to that achieved in pure water.

To further investigate the effect of encapsulated guest molecules on the morphologies of the I_3K self-assemblies, AFM measurements were performed with variation in the molar ratio (δ) of model drugs to peptide hosts on the self-assembled peptide nanostructures (Fig. 5). At a relatively low ratio ($\delta = 0.05$), well-defined nanotubes could be observed and all of the MO molecules were expected to be entrapped in the self-assembled nanotubes with a diameter of 8.6 nm (Fig. 5a). As the molar ratios were increased to 0.1, no noticeable morphology of the self-assemblies was observed; however, the diameters of the nanotubes decreased to 6.4 nm (Fig. 5b). As the molar ratio was further increased to 0.2, the diameters of the self-assembled nanostructures decreased to 3.4 nm (Fig. 5c). It is explained that the introduction of negatively-charged MO molecules may neutralize the positive charges on the surfaces of I_3K nanotubes, which cause the contract of the self-assemblies. A similar phenomenon was observed when low OR concentrations were introduced to the self-assembled system (Fig. 5d and e). However, the morphologies and sizes of self-assembled nanostructures were found to be affected at high molar ratios (Fig. 5f). More OR molecules encapsulated in I_3K self-assemblies could break the elongated nanotubes into short tubular segments, which are the dominant species in the solution with diameters of 2.3 nm and lengths of approximately 500 nm. It should be noted that, even though the introduction of guest molecules change the morphologies of peptide nanotubes, the main secondary structure of nanotubes remains essentially (*vide infra*).

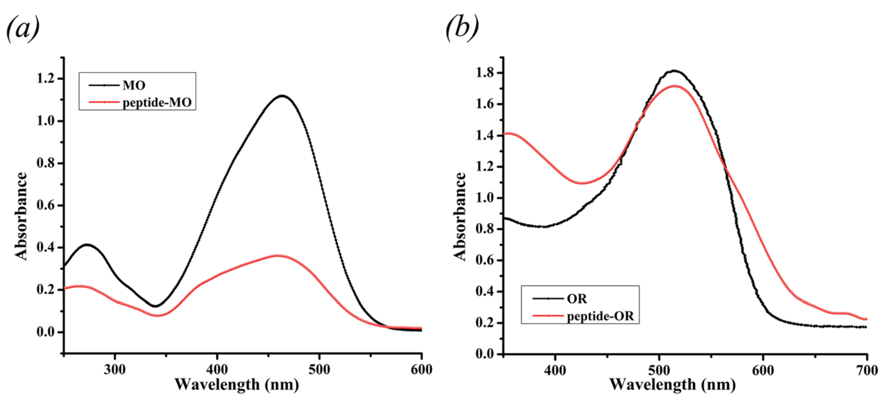

Fig. 4 UV-Vis absorption spectra of encapsulated model drugs in I_3K peptide solutions: (a) MO and (b) OR.

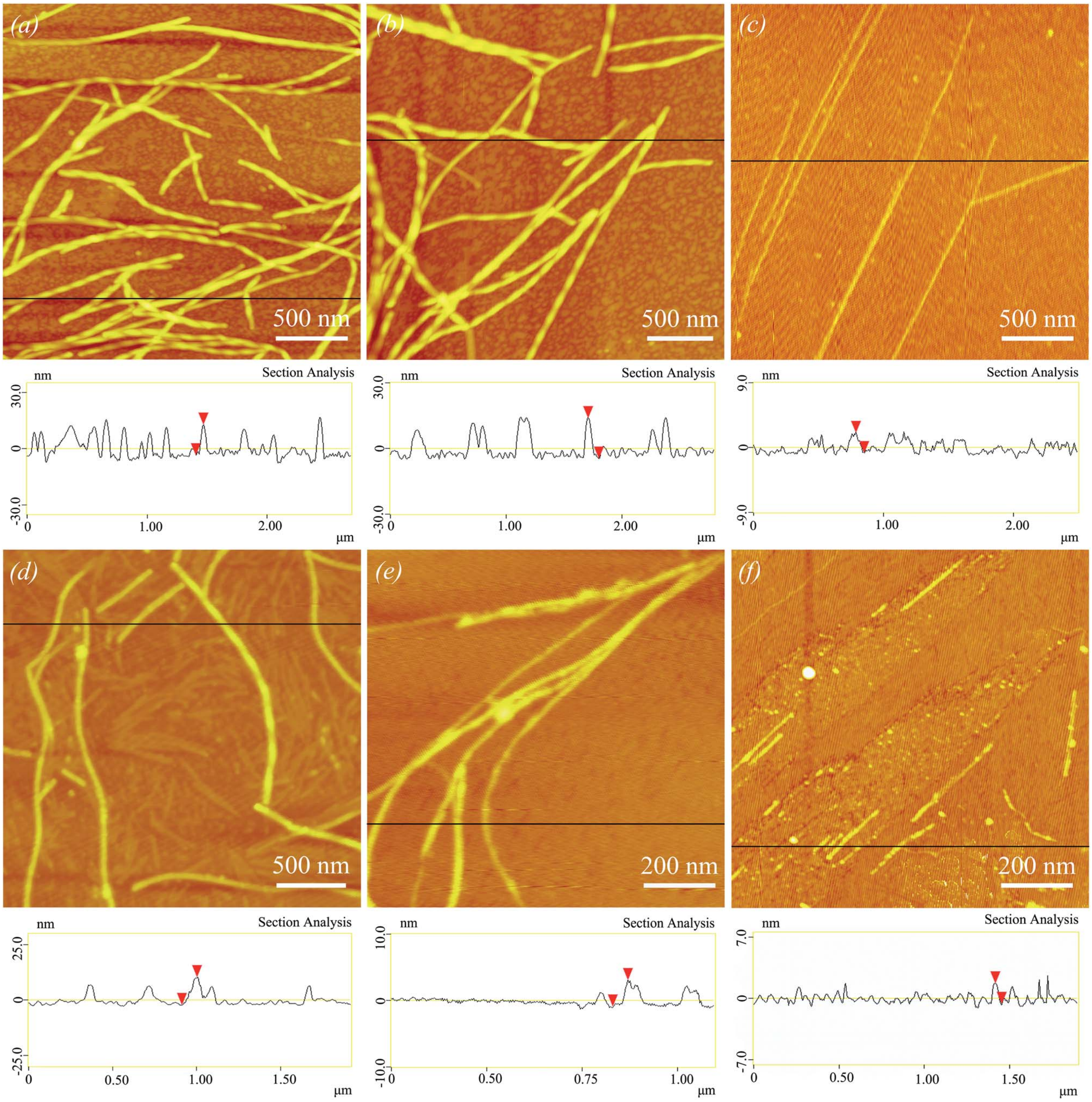

Fig. 5 Effects of drug concentration on peptide nanostructures. AFM height images of MO entrapped in I_3K self-assembled nanostructures at different ratio: (a) $\delta = 0.05$, (b) $\delta = 0.1$, and (c) $\delta = 0.2$. AFM height images of OR entrapped in I_3K self-assembled nanostructures at different ratio: (d) $\delta = 0.05$, (e) $\delta = 0.1$, and (f) $\delta = 0.2$.

3.3 Secondary structure analysis

CD measurements were carried out to investigate the effects of drugs on peptide conformation in the self-assembled nanostructures at various molar ratios. As shown in Fig. 6a, a solution of I_3K in pure water yields a CD spectrum with a negative minimum value at approximately 220 nm, revealing the predominance of β-sheet conformation associated with the self-assembled system. Isoleucine likely promotes the growth of nanotubular morphologies, and hydrogen bonding commonly facilitates short peptide self-assembly.[35,46] As a result, hydrogen bonding dominantly regulates I_3K nanostructures. The growth of β-sheet hydrogen bonding along the axial length possibly directs the fabrication of self-assembled nanotubes. This result indicated the combined interplay between hydrogen bonding and hydrophobic interactions. The introduction of MO and OR to the I_3K nanotubes did not change significantly the CD spectra (with a negative peak at 217 nm to 223 nm), revealing the remaining of the β-sheet structures (Fig. 6b and c). However, with the increase of molar ration δ, the strength of CD spectra weakened, indicative of decreased stability of the self-

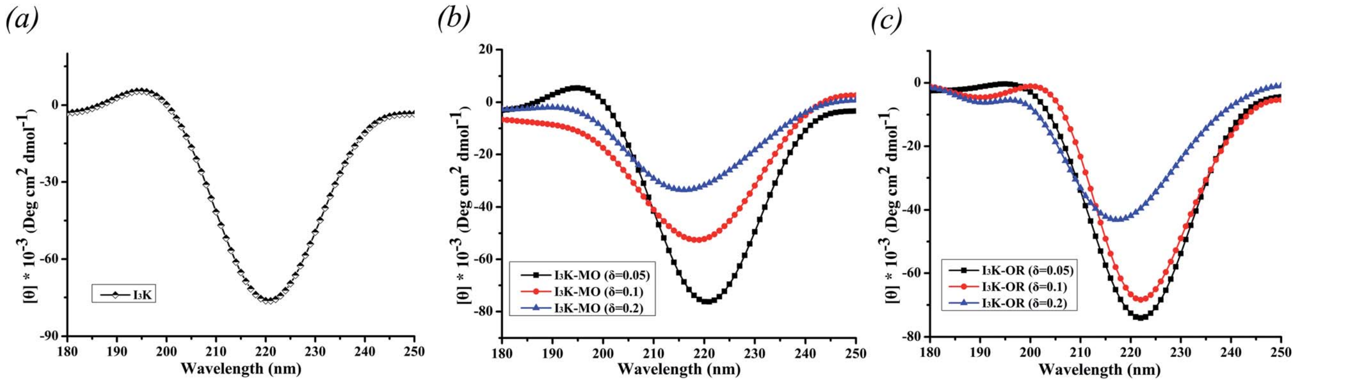

Fig. 6 CD spectra of (a) I_3K, (b) I_3K/MO, and (c) I_3K/OR, respectively.

assembled nanotubes, which was consistent with the AFM measurements.

3.4 *In vitro* release of encapsulated model drug from I_3K self-assemblies

Hydrophobic model drugs cannot be spontaneously released because of their poor water solubility. Thus, the *in vivo* release of OR is primarily dependent on the degradation kinetics of self-assembled peptides.

The entrapment of anionic model compounds was mainly dependent on the electrostatic interactions between positively-charged lysine in I_3K and negatively-charged guest molecules at physiological pH. Therefore, the change of the charging state of either lysine residue or guest molecules would result in the variation of electrostatic interactions between them, which may lead to a change in the releasing kinetics of loaded guest molecules. For example, the pK_a of the side chains of PLL was approximately 9.0–10.0, and MO had a pK_a of approximately 3.4. An increase in the solution pH from 7.4 to 11.0 could gradually convert the side chain of PLL from a protonated form to a deprotonated form while the charging state of MO remains unchanged, weakening electrostatic interactions between the polymer host and anionic guest molecules and thereby accelerate the releasing rate of guest molecules. On the other hand, a decrease in the solution pH from 7.4 to 2.0 could gradually convert the charge of MO from being negative to neutral,[47] while PLL remains positively-charged, which could also weaken electrostatic interactions, speeding up the releasing rate of guest molecules.

To study the releasing kinetics of entrapped MO from I_3K nanotubes, the drug-loaded nanotube solution was transferred to a dialysis bag and dialyzed against the solution at different pH conditions (pH 2.0 to 11.0). The cumulative release profiles of peptide-encapsulated MO under different pH conditions are shown in Fig. 7. The encapsulated model drug exhibited a relatively high stability under physiological pH, and the cumulative release was less than 10% after 7 days. The entrapped MO demonstrated an accelerated release when the pH is either increased or decreased. For example, the cumulative release of MO was approximately 22% of MO was released after 7 days when pH was regulated to 10.0. Furthermore, more than 25% of MO was released from I_3K self-assemblies after 7 days when pH was further increased to 11.0. The fast releasing kinetics at high pH is consistent with the deprotonation of lysine side chains, and 31% of MO was released from I_3K nanotubes after 7 days when the solution pH was decreased to 3.0. The fastest release rate was observed and the cumulative release was more than 38% after 7 days when the solution pH was further decreased to 2.0. The accelerated releasing rate of MO from I_3K nanotubes under low pH is the result of the charge conversion of MO from being negative to neutral. The changes in the charging state of either lysine chains or the guest compound likely lead to a variation in electrostatic interactions between these substances, which may lead to a change in the releasing kinetics of the loaded guest compound. Therefore, the pH-responsive release of the encapsulated model drugs can be achieved *via* the pH-responsive charge switching in either a host peptide or an entrapped guest compound.

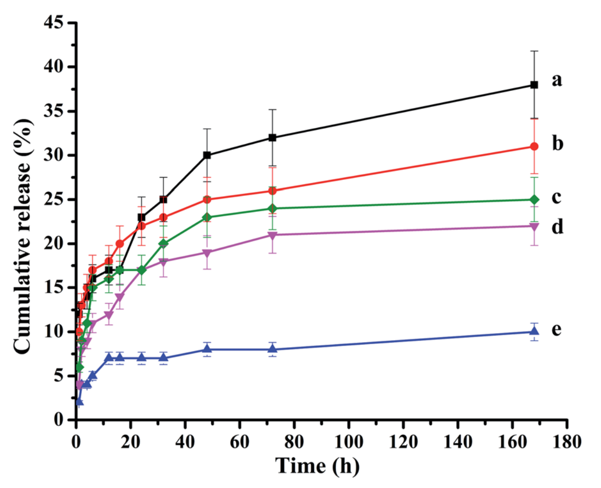

Fig. 7 Release of loaded MO from I_3K self-assemblies at various pH levels. Curves a, b, c, d, and e correspond to pH levels of 2.0, 3.0, 11.0, 10.0, and 7.4, respectively. The errors of the measurements are in the range of ±10%.

4. Conclusions

The self-assembly of the short amphiphilic peptide I_3K into nanotubes and its potential application in drug delivery nanocarrier have been investigated. The short peptide I_3K self-assembles to form well-ordered nanotubes in aqueous solution. The dynamic process of I_3K peptide self-assembly started with nanotubular segments and then to helical nanostructures, followed by the final well-ordered and highly homogeneous nanotubes after one week of incubation. The encapsulation properties of the self-assembled peptide nanotubes have been evaluated using MO as anionic hydrophilic model compounds and OR as hydrophobic guest molecules. I_3K self-assemblies demonstrated an efficient encapsulation of model drugs at neutral pH. The loading capacity of self-assembled peptide nanotubes toward MO and OR could reach up to 12% and 8%, respectively. The encapsulated hydrophilic drugs exhibited a relatively high temporal stability and revealed sustained release at physiological pH. A decrease or increase in pH could change the charging state of the lysine units in the short peptide or entrapped guest molecules, resulting in a pH-responsive release of entrapped model drugs. Facile synthesis and non-toxicity of I_3K, well-defined self-assemblies, efficient encapsulation, and sustained pH-responsive releasing properties make I_3K nanotube potential nanocarriers for the controlled release of drugs.

Acknowledgements

This work was supported by the National Natural Science Foundation of China (20871080, 50973058), the Team Project of the Natural Science Foundation of Guangdong Province (9351503102000001), and Innovation Team Construction Project of Shantou University (ITC11002).

References

1 E. Soussan, S. Cassel, M. Blanzat and I. Rico-Lattes, *Angew. Chem., Int. Ed.*, 2009, **48**, 274–288.
2 P. T. Hammond, *ACS Nano*, 2011, **5**, 681–684.
3 S.-M. Lee and S. T. Nguyen, *Macromolecules*, 2013, **46**, 9169–9180.
4 Q. Duan, Y. Cao, Y. Li, X. Hu, T. Xiao, C. Lin, Y. Pan and L. Wang, *J. Am. Chem. Soc.*, 2013, **135**, 10542–10549.
5 V. P. Torchilin, *Curr. Drug Delivery*, 2005, **2**, 319–327.
6 S. Y. Fung, H. Yang, P. T. Bhola, P. Sadatmousavi, E. Muzar, M. Liu and P. Chen, *Adv. Funct. Mater.*, 2009, **19**, 74–83.
7 G. Bonacucina, M. Cespi, M. Misici-Falzi and G. F. Palmieri, *J. Pharm. Sci.*, 2009, **98**, 1–42.
8 T. Shimizu, M. Masuda and H. Minamikawa, *Chem. Rev.*, 2005, **105**, 1401–1444.
9 X. Zhao, F. Pan, H. Xu, M. Yaseen, H. Shan, C. A. Hauser, S. Zhang and J. R. Lu, *Chem. Soc. Rev.*, 2010, **39**, 3480–3498.
10 I. Hamley, *Soft Matter*, 2011, **7**, 4122–4138.
11 H. Hosseinkhani, P.-D. Hong and D.-S. Yu, *Chem. Rev.*, 2013, **113**, 4837–4861.
12 A. Rösler, G. W. Vandermeulen and H.-A. Klok, *Adv. Drug Delivery Rev.*, 2012, **64**, 270–279.
13 H. Xu, J. Wang, S. Han, J. Wang, D. Yu, H. Zhang, D. Xia, X. Zhao, T. A. Waigh and J. R. Lu, *Langmuir*, 2009, **25**, 4115–4123.
14 Z. Luo and S. Zhang, *Chem. Soc. Rev.*, 2012, **41**, 4736–4754.
15 H. Liu, J. Chen, Q. Shen, W. Fu and W. Wu, *Mol. Pharm.*, 2010, **7**, 1985–1994.
16 G. Verma and P. Hassan, *Phys. Chem. Chem. Phys.*, 2013, **15**, 17016–17028.
17 H. Shao and J. R. Parquette, *Angew. Chem., Int. Ed.*, 2009, **48**, 2525–2528.
18 S. N. Barnaby, K. R. Fath, A. Tsiola and I. A. Banerjee, *Colloids Surf., B*, 2012, **95**, 154–161.
19 X. Xu, Y. Li, H. Li, R. Liu, M. Sheng, B. He and Z. Gu, *Small*, 2014, **10**, 1133–1140.
20 U. Khoe, Y. Yang and S. Zhang, *Macromol. Biosci.*, 2008, **8**, 1060–1067.
21 Q. Meng, Y. Kou, X. Ma, Y. Liang, L. Guo, C. Ni and K. Liu, *Langmuir*, 2012, **28**, 5017–5022.
22 S. Wang, J. Xue, X. Ge, H. Fan, H. Xu and J. R. Lu, *Chem. Commun.*, 2012, **48**, 9415–9417.
23 S. Han, S. Cao, Y. Wang, J. Wang, D. Xia, H. Xu, X. Zhao and J. R. Lu, *Chem.–Eur. J.*, 2011, **17**, 13095–13102.
24 C. Chen, F. Pan, S. Zhang, J. Hu, M. Cao, J. Wang, H. Xu, X. Zhao and J. R. Lu, *Biomacromolecules*, 2010, **11**, 402–411.
25 H. Cui, M. J. Webber and S. I. Stupp, *Biopolymers*, 2010, **94**, 1–18.
26 H. Xu, C. Chen, J. Hu, P. Zhou, P. Zeng, C. Cao and J. R. Lu, *Biomaterials*, 2013, **34**, 2731–2737.
27 Q. Wang, J. Yu, X. Zhang, D. Liu, J. Zheng, Y. Pan and Y. Lin, *RSC Adv.*, 2013, **3**, 2784–2793.
28 Q. Wang, J. Yu, J. Zheng, D. Liu, F. Jiang, X. Zhang and W. Li, *RSC Adv.*, 2013, **3**, 15955–15965.
29 N. Kameta, H. Minamikawa and M. Masuda, *Soft Matter*, 2011, **7**, 4539–4561.
30 J. Wang, S. Han, G. Meng, H. Xu, D. Xia, X. Zhao, R. Schweins and J. R. Lu, *Soft Matter*, 2009, **5**, 3870–3878.
31 M. Cao, Y. Wang, X. Ge, C. Cao, J. Wang, H. Xu, D. Xia, X. Zhao and J. R. Lu, *J. Phys. Chem. B*, 2011, **115**, 11862–11871.
32 Y. Yan, J. Li, J. Zheng, Y. Pan, J. Wang, X. He, L. Zhang and D. Liu, *Colloids Surf., B*, 2012, **95**, 137–143.
33 M. Gale, M. S. Pollanen, P. Markiewicz and M. C. Goh, *Biophys. J.*, 1995, **68**, 2124–2128.
34 K. Lu, J. Jacob, P. Thiyagarajan, V. P. Conticello and D. G. Lynn, *J. Am. Chem. Soc.*, 2003, **125**, 6391–6393.
35 S. E. Paramonov, H.-W. Jun and J. D. Hartgerink, *J. Am. Chem. Soc.*, 2006, **128**, 7291–7298.
36 M. Krysmann, V. Castelletto, J. McKendrick, L. Clifton, P. Harris and S. King, *Langmuir*, 2008, **24**, 8158–8162.
37 H. Xu, Y. Wang, X. Ge, S. Han, S. Wang, P. Zhou, H. Shan, X. Zhao and J. R. Lu, *Chem. Mater.*, 2010, **22**, 5165–5173.
38 C. W. Fishwick, A. J. Beevers, L. M. Carrick, C. D. Whitehouse, A. Aggeli and N. Boden, *Nano Lett.*, 2003, **3**, 1475–1479.
39 G. John, J. H. Jung, H. Minamikawa, K. Yoshida and T. Shimizu, *Chem.–Eur. J.*, 2002, **8**, 5494–5500.

40 A. Aggeli, I. Nyrkova, M. Bell, R. Harding, L. Carrick, T. McLeish, A. Semenov and N. Boden, *Proc. Natl. Acad. Sci. U. S. A.*, 2001, **98**, 11857–11862.
41 S. Wang, X. Ge, J. Xue, H. Fan, L. Mu, Y. Li, H. Xu and J. R. Lu, *Chem. Mater.*, 2011, **23**, 2466–2474.
42 E. Gazit, *Chem. Soc. Rev.*, 2007, **36**, 1263–1269.
43 H. Wang and Z. Yang, *Nanoscale*, 2012, **4**, 5259–5267.
44 W. She, N. Li, K. Luo, C. Guo, G. Wang, Y. Geng and Z. Gu, *Biomaterials*, 2013, **34**, 1613–1623.
45 X. Zeng, J. Li, J. Zheng, Y. Pan, J. Wang, L. Zhang, X. He and D. Liu, *Colloids Surf., B*, 2012, **94**, 324–332.
46 H. A. Arfmann, R. Labitzke and K. Wagner, *Biopolymers*, 1977, **16**, 1815–1826.
47 H. Tian, X. Chen, H. Lin, C. Deng, P. Zhang, Y. Wei and X. Jing, *Chem.–Eur. J.*, 2006, **12**, 4305–4312.